metals

MDPI

Article

Tensile Behavior and Microstructure Evolution of an Extruded 6082 Aluminum Alloy Sheet at High Temperatures

Sawei Qiu [1,2], Erli Xia [1,2], Limei Liu [1,2], Tuo Ye [1,2], Jie Liu [1], Jian Tang [1], Wei Liu [1,2] and Yuanzhi Wu [1,2,*]

[1] School of Intelligent Manufacturing and Mechanical Engineering, Hunan Institute of Technology, Hengyang 421002, China; 2022001005@hnit.edu.cn (S.Q.); 2021001046@hnit.edu.cn (E.X.); 2017001002@hnit.edu.cn (T.Y.)
[2] Research Institute of Automobile Parts Technology, Hunan Institute of Technology, Hengyang 421002, China
* Correspondence: 2013001767@hnit.edu.cn

Abstract: The hot tensile behavior of an extruded 6082 alloy sheet at varying temperatures and strain rates was investigated by a Gleeble3500 thermal simulation testing machine. The optical microscope (OM), scanning electron microscope (SEM), transmission electron microscopy (TEM) and X-ray diffraction (XRD) were applied to observe the microstructure evolution. It is found that the flow stress of the studied alloy declines with increasing deformation temperature. When deformed at high temperatures, the density of dislocation decreases obviously. In addition, precipitate coarsening occurs, resulting in a decrease in deformation resistance. The dimple number of the fracture samples increases with temperature and the size of the dimple becomes deeper, exhibiting an excellent plasticity. The 6082 sheet presents anisotropy of mechanical behavior at 300 °C, this can be attributed to the fibrous grain and the Brass component {011}<211>. The anisotropic behavior seems to be slighter with an increase in temperature. No obvious anisotropic behavior was found when tensiled at 400 °C. Because it is easier to activate the slip system at elevated temperatures, meanwhile, the recrystallization begins to occur at 400 °C.

Keywords: high-temperature tensile; 6082 sheet; microstructure; anisotropy

check for updates

Citation: Qiu, S.; Xia, E.; Liu, L.; Ye, T.; Liu, J.; Tang, J.; Liu, W.; Wu, Y. Tensile Behavior and Microstructure Evolution of an Extruded 6082 Aluminum Alloy Sheet at High Temperatures. *Metals* **2024**, *14*, 7. https://doi.org/10.3390/met14010007

Academic Editor: Mark E. Schlesinger

Received: 29 November 2023
Revised: 18 December 2023
Accepted: 19 December 2023
Published: 20 December 2023

Copyright: © 2023 by the authors. Licensee MDPI, Basel, Switzerland. This article is an open access article distributed under the terms and conditions of the Creative Commons Attribution (CC BY) license (https://creativecommons.org/licenses/by/4.0/).

1. Introduction

When compared to non-ferrous metals, low density is the most incomparable advantage of aluminum and its alloy [1]. Aluminum alloys provide the most feasible methods to achieve lightweight components or parts. In addition, aluminum alloys display desirable mechanical properties [2]. Therefore, aluminum products have widespread application in the areas of aerospace, transportation and navigation [3–5]. A 6082 aluminum alloy is a kind of the most popular aluminum alloys, which has been well promoted for various applications in lightweight components or parts [6]. The major alloying elements of 6082 alloy are magnesium, silicon and copper, and this alloy can offer favorable strength, excellent corrosion resistance, good resistance to fatigue and outstanding recyclability [7]. The increasing use of this alloy is based on the processes of heat treatments and plastic deformation with considerable mechanical properties [8–10].

At room temperature, the plasticity of the 6082 alloy is far from expected and it is difficult to meet the requirements of forming conditions. Therefore, hot forming is generally used, such as hot extrusion, hot forging, hot rolling and so on. Noga et al. [11] produced a 6082 alloy profile by hot extrusion process, which owns a satisfied quality and mechanical properties. Peruš et al. [12] made optimization of extrusion parameters to improve the yield strength and elongation of the 6082 alloy profile. HUA et al. [13] proposed a novel forging process of 6082 alloy, this method was proved to effectively promote productivity without losing the comprehensive performance. Noga et al. [14] conducted joining tests of 6082-T6 alloy, and the results show that electron beam welding joints have better strength properties; however, a reduction of elongation for both joints was observed. As the forming

temperature increases, the material deformation resistance declines, and the formability of aluminum alloy is greatly improved, displaying the advantages of high forming accuracy and high production efficiency.

During the hot forming process, the materials undergo substantial plastic deformation at elevated temperatures, the microstructure would take a great change. Aluminum alloy is a kind of high-stacking fault energy material, dynamic recovery and dynamic recrystallization is a common phenomenon. Hu et al. [15] compressed the 6082 alloys at 350–500 °C and 0.01–5 s^{-1}, a substantial of subgrain boundaries were found after deformation. Li et al. [16] conducted compression tests of 6082 alloy at elevated temperatures, they observed that the dislocations took a great change and different evolution under various conditions, which directly affects the mechanical properties of 6082 alloy. Additionally, the precipitates undergo giant evolution. Yang et al. [17] explored the deformation behavior and microstructure of Al-Mg-Si alloy, and they concluded that coarsening dynamic precipitates is the main reason for dynamic softening. It can be concluded that during the hot deformation, the grain, dislocation and precipitate have taken a significant evolution. In turn, it is widely accepted that the microstructure has a determining effect on the properties of the material [6,18]. Zheng et al. [19] carried out hot tensile tests of 6082 alloy. The strength of the studied alloy declines with temperature and decreasing strain rate. Zhao et al. [20] conducted a compression test of the 6082 alloy at 400–535 °C and 0.1–10 s^{-1}. The results indicate that the compressive stress is inversely proportional to temperature and, at the same time, directly proportional to the strain rate. Xu et al. [21] investigated the formability of the 6082 alloy, at temperatures of 200 °C, 300 °C and 400 °C. The strength drops down with temperature, and it is worth noting that the forming resistance falls down sharply at 300 °C.

In addition to the softening behavior of the material, it is acknowledged that the aluminum alloy displays obvious anisotropy after a server deformation. Chen et al. [22] tested the mechanical response of the 6082 alloy at strain rates 1–10^3 s^{-1}, the alloy with fibrous grains exhibits anisotropic mechanical properties, and samples with 45° respect to the extrusion axle have the poorest stress. Chakraborty et al. [23] conducted a tensile test of AA7475 alloy, and the results indicate that the yield strengths of rolling direction samples are the highest at room temperature; however, the anisotropy becomes less evident at higher temperatures. Barnwal et al. [24] found that the 6061 alloy sheet processed by severe rolling deformation displays a prominent anisotropy. The sample along the rolling direction has the highest tensile strength. They also identify that the anisotropy is decisive for the subsequent forming process of the sheet. After forming processes such as rolling and extrusion, the components or parts exhibit characteristics of uneven microstructure and anisotropic properties, ultimately resulting in uneven processing performance of the material at different forming angles. Therefore, accurately predicting the anisotropic behavior of materials is of great significance for selecting processing parameters reasonably and achieving high-quality processing of aluminum alloys.

Fan et al. [25] provided evidence that the rolling texture and the density of grain boundary are the dominant aspects that lead to differences in the yield strength of the samples in various directions. Yang et al. [26] presented that the anisotropy of the extruded alloy bar can be explained by the elongated grains as well as the {112}<111> and {110}<111> textures formed during extrusion. Ye et al. [27] explored the compressive behavior of an extruded bar, and the results show that the fiber grains are responsible for the highest strength in the extrusion direction. Meanwhile, the Schmid factor is calculated and discussed, and it is proven that the deformation texture has a great influence on the anisotropy. In total, the main reasons for the anisotropic tensile properties are the following: (a) the characteristics of crystallographic texture; (b) the morphology of grains; and (c) the distribution of the main precipitate. Most of the aluminum alloy parts are produced through plastic deformation. Therefore, figuring out the mechanism of anisotropy is profound in order to widen the application of metals.

As the manufacturing industry develops rapidly, the requirements for material processing quality and service performance are becoming increasingly stringent. Despite the

numerous studies reported on the influences of the strain degree, deformation temperature and strain rate on the deformation response of aluminum alloy, the exploration of deformation behavior and microstructural mechanism for 6082 alloy at elevated temperature is limited. To figure out the relationship between tensile behavior and microstructure mechanism will provide experimental and theoretical data for the hot forming process design and optimization.

2. Experimental

2.1. Materials

The extruded 6082 alloy studied in this research is in the form of a sheet with initial dimensions of 100 mm in width and 2 mm in thickness. The extrusion parameters are listed in Table 1. The chemical compositions of the sheet are listed in Table 2.

Table 1. The extrusion process parameters of 6082 alloy sheet.

Extrusion Speed	Billet Temperature	Die Temperature	Container Temperature	Extrusion Ratio
2 mm/s	520 °C	467 °C	450 °C	21.2

Table 2. Chemical composition of 6082 sheet.

Element	Si	Fe	Cu	Mn	Mg	Cr	Zn	Ti	Al
wt%	0.89	0.2	0.1	0.43	0.75	0.1	0.02	0.09	Balance

2.2. High-Temperature Tensile Test

As illustrated in (Figure 1a), hot tensile test samples were machined from the sheet with 0°, 45° or 90° along the extrusion direction (ED). The size of the sample is shown in (Figure 1b). The hot tension was conducted in a Gleeble3500 machine (DSI, St. Paul, MN, USA), the heating rate was 5 °C/s, and, when the target temperature was obtained, the samples were held for 2 min. The tensile temperatures are 300 °C and 400 °C, and the strain rates are 0.1 s^{-1}, 0.01 s^{-1} and 0.001 s^{-1}. Once the tensions were finished, the samples were immediately water cooled to freeze the microstructures.

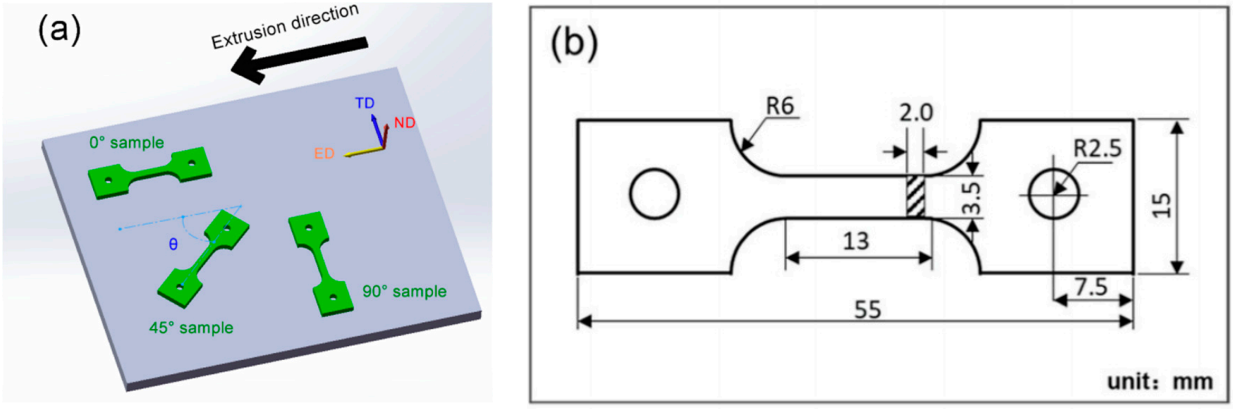

Figure 1. (**a**) Sample position, and (**b**) the dimension of the sample (unit: mm).

2.3. Characterization

The optical observation samples were extracted from the fracture samples demonstrated in (Figure 2). The samples were ground and polished to obtain a mirror surface. Then, the electrolytic etching was applied to the microstructure, the etching solution was 120 mL water and 4 mL HBF_4, the etching voltage was 18 V, the etching time ranged from 1 to 3 min, and microstructural observation was performed using an optical microscope

(AX10, Zeiss, Oberkochen, Baden-Württemberg, Germany). The SEM (FEI, Hillsboro, OR, USA) was adopted to observe the fracture morphology. TEM observation samples with a thickness of 0.5 mm were obtained by wire electrical discharge machining process. Then, the slice was ground to 70 μm, the slice was punched into a round plate with a diameter of 3 mm, and subjected to chemical thinning and perforation by double spraying on the MIP-1A magnetic-driven double spraying thinning instrument. The microstructure was then observed under the Talos F200X (FEI, Hillsboro, OR, USA). X-ray diffractometer (BRUKER, Billerica, MA, USA) was used to conduct texture measurement, the voltage is 40 kV, and the current is 40 mA. The reflection method was used to measure the incomplete polar maps (0°~70°) of {111}, {200} and {220} planes, and then the standard polar map was synthesized, and the orientation distribution function ODF map was calculated.

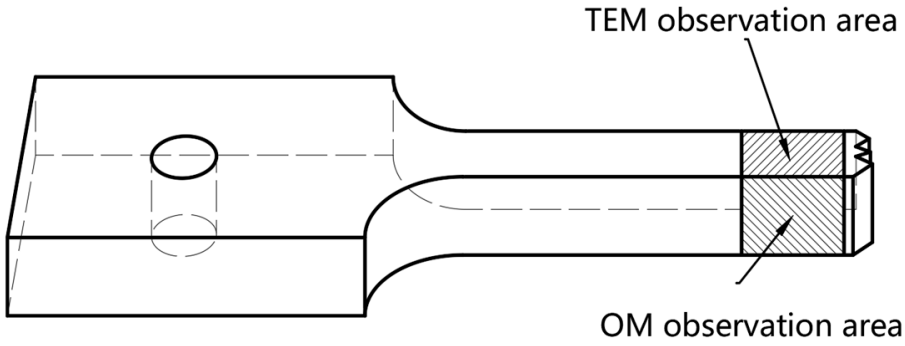

Figure 2. The characterization area of the sample.

3. Results and Analysis

3.1. True Stress–True Strain Curves

As shown in Figure 3, the true stress–true strain curves of 6082 sheets under experimental parameters of 300 °C and 400 °C and strain rates of 10^{-3} s^{-1}, 10^{-2} s^{-1} and 10^{-1} s^{-1} are obtained. During hot tension, the true stress first climbs up sharply with the increase in strain, and then slowly increases before hitting the maximum value. Finally, the true stress begins to decrease with increasing strain. This is because during the early period of tension, the dislocation density multiplies significantly, the interaction between dislocations promotes the motion impedance of dislocations, and the sample undergoes work-hardening effect. Then, the yielding phenomenon of the materials is observed. As deformation continues, dynamic recovery or dynamic recrystallization will take place. When peak stress is obtained, the effects of work hardening and dynamic softening keep a dynamic balance condition. Subsequently, dynamic softening leads to a dominant place in deformation, and the stress of the sample declines with increasing strain, ultimately leading to failure. Comparing the curves under different conditions, it was found that the stress declines with temperature and increases with strain rate. For example, as shown in Table 3, when deformed at 300 °C, 0.001 s^{-1}, the peak stress of the 0° direction sample is 114 MPa, and, as the temperature rises to 400 °C, the peak stress drops to 30 MPa. However, when the strain rate climbs up to 0.1^{-1} s^{-1}, the corresponding peak stress is 51 MPa. Increasing temperature contributes to the softening effect of dynamic recovery or dynamic recrystallization of the material, leading to a drop in dislocation density. Meanwhile, the solubility of the second phase is increased. The resistance of the slip declines, resulting in a fall of deformation resistance. Moreover, the increasing strain rate could fortify the work-hardening effect, the softening rate caused by dynamic recovery or recrystallization is insufficient to offset the work-hardening rate caused by strain rate strengthening; therefore, a rise in stress is found. It is worth noting that a low strain rate and high temperature are likely to trigger an earlier flow-softening behavior at a low strain degree, and the more obvious softening effect.

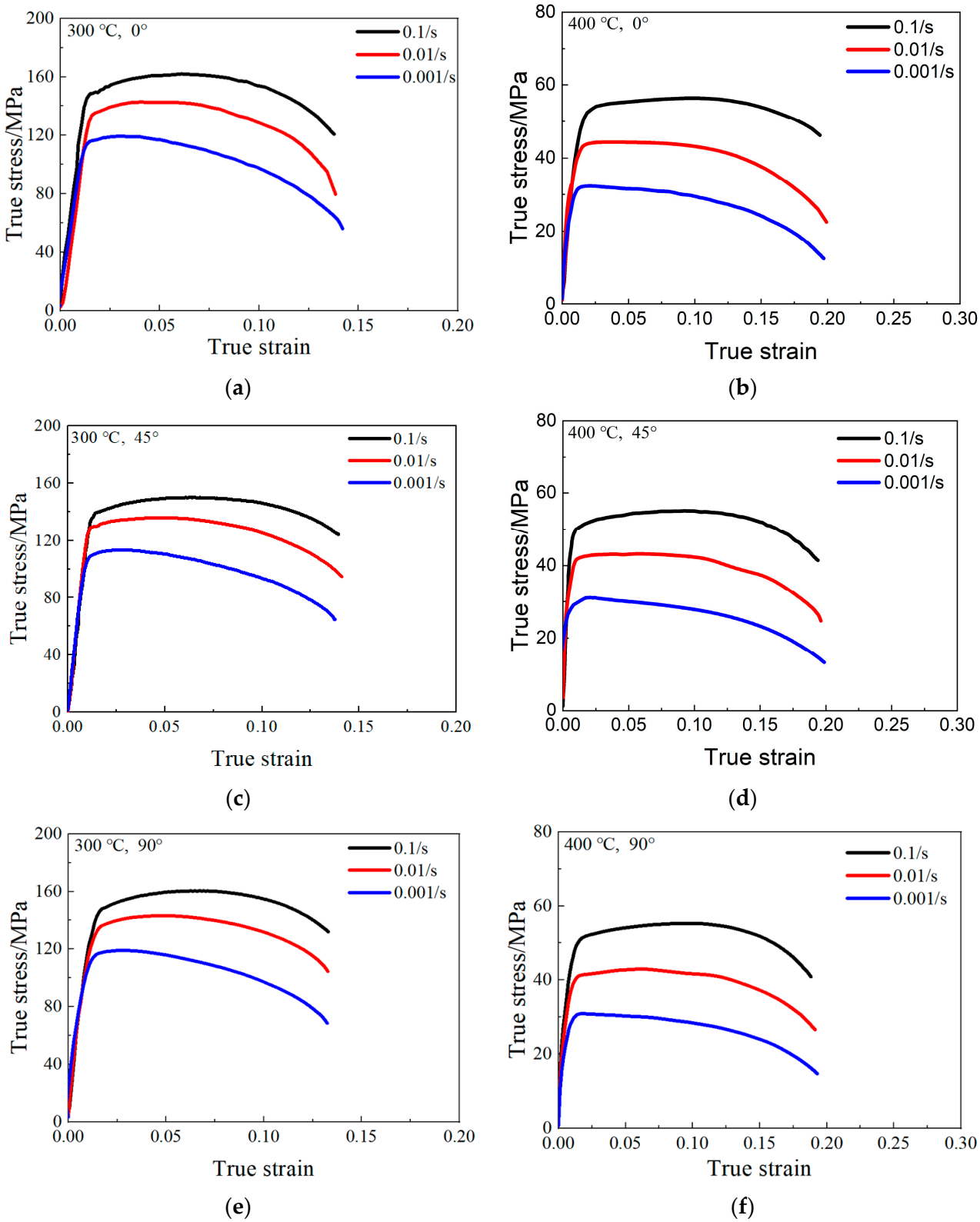

Figure 3. True stress–true strain curves of samples at different tensile conditions: (**a**) 0° 300 °C, (**b**) 0° 400 °C, (**c**) 45° 300 °C, (**d**) 45° 400 °C, (**e**) 90° 300 °C, (**f**) 90° 400 °C.

Table 3. The mechanical properties of 6082-T6 sheet.

Temperature (°C)	Direction (°)	Strain Rate (s^{-1})	Yield Strength (MPa)	Tensile Strength (MPa)	Elongation (%)
300	0	0.1	146	163	16.5
		0.01	133	143	17.3
		0.001	114	120	18.1
	45	0.1	138	151	17.2
		0.01	129	136	17.9
		0.001	107	114	18.4
	90	0.1	146	160	16.6
		0.01	134	142	17.5
		0.001	115	118	18.0
400	0	0.1	53	56	22.1
		0.01	42	44	23.8
		0.001	30	32	24.9
	45	0.1	52	55	22.5
		0.01	40	43	24.2
		0.001	28	31	24.8
	90	0.1	51	55	22.3
		0.01	41	42	23.9
		0.001	29	31	24.7

3.2. Anisotropic Mechanical Properties

The peak stress of the samples cut from various orientations is shown in Figure 4. In general, at the deformation temperature of 300 °C, the peak stress of 0° samples is the highest, the peak stress of 90° samples is slightly lower than that of 0° samples, and the stress level of 45° samples is the lowest. For example, as shown in Figure 4a, at 300 °C, 0.1 s^{-1}, the peak stresses for 0°, 45° and 90° samples are 146 MPa, 138 MPa and 146 MPa, respectively. Similar results have been reported in previous studies, which can be explained by fibrous grains and deformation texture [28,29]. However, as the tensile temperature rises to 400 °C, there is no obvious anisotropic mechanical behavior, and the flow stresses of different direction samples are at the same level. For example, as shown in Figure 4b, at 400 °C, 0.001 s^{-1}, the peak stresses for 0°, 45° and 90° samples are around 31 MPa. Higher temperature provides sufficient energy to facilitate the recovery and recrystallization processes, the density of dislocation decreases sharply, and the slip is easier to activate; meanwhile, the deformed textures in the original sheet transit to recrystallized texture [30,31]. Therefore, the anisotropy has been weakened or even eliminated.

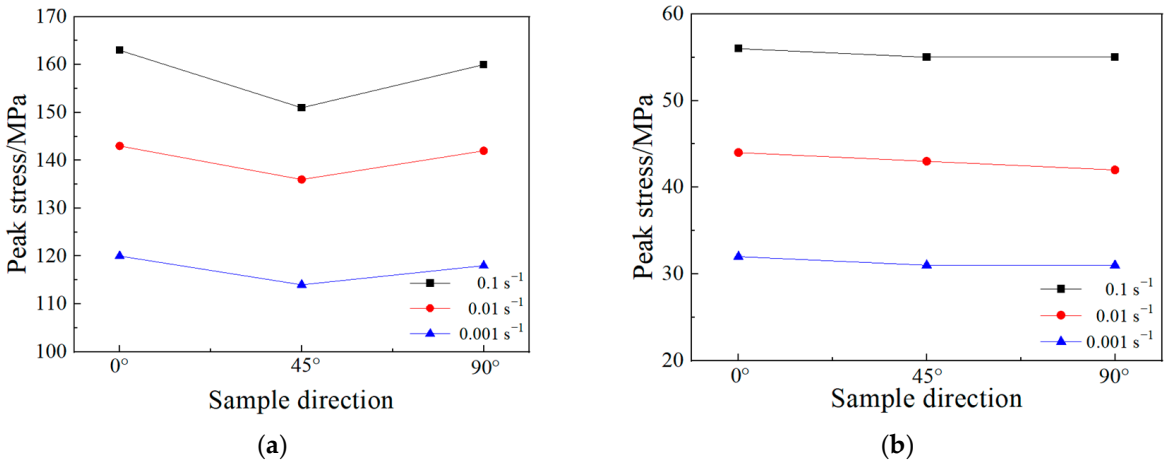

Figure 4. Peak stress as a function of sample direction: (**a**) 300 °C, (**b**) 400 °C.

3.3. Fracture Observation

Figure 5 shows the macroscopic fracture surfaces of 6082 aluminum alloy samples under various tensile conditions. From Figure 5c–e, it is clear that under hot tensile conditions, aluminum alloy tensile samples in all three directions exhibit a significant necking phenomenon, exhibiting excellent elongation. According to Figure 5b,c, under a constant temperature condition (400 °C), the lower the tensile strain rate, the smaller cross section of the fracture, the more obvious necking of the sample, and the better the elongation of this material. As shown in Figure 5a,b, it is clear that when the hot tensile is at 0.1 s^{-1}, the cross section of the fracture is smaller at a higher temperature, and the necking phenomenon of the material is more obvious, showing a greater elongation.

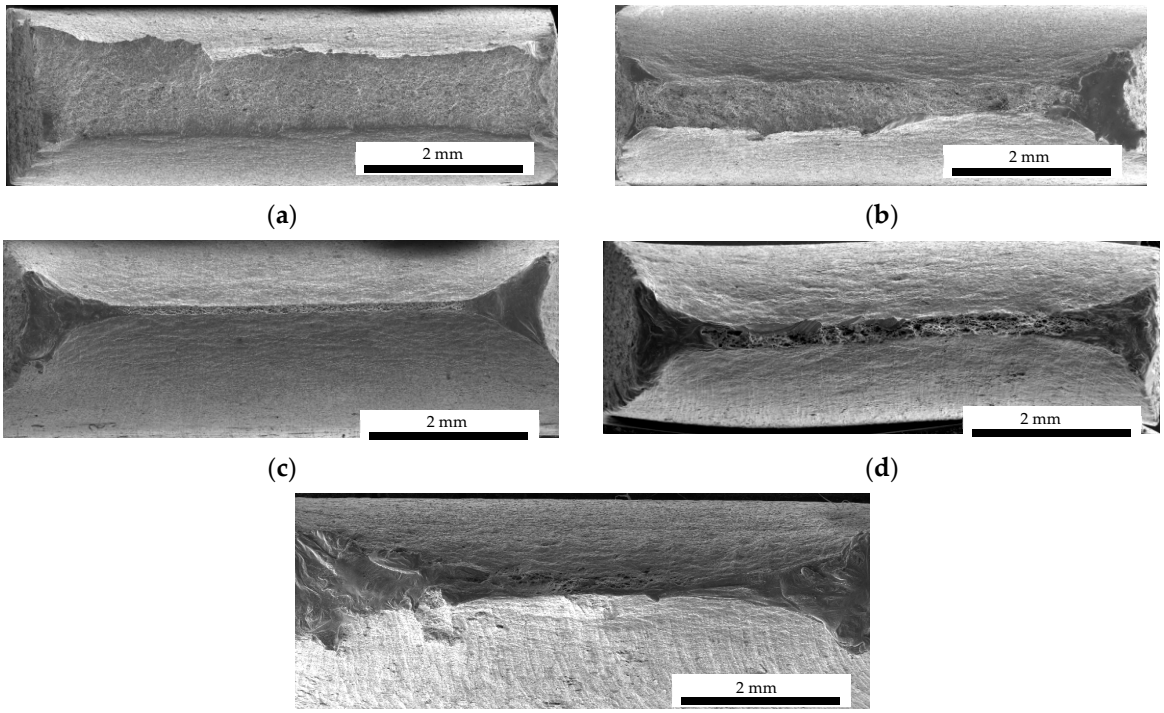

Figure 5. Tensile macroscopic fracture under different deformation conditions: (**a**) 0° 300 °C 0.1 s^{-1}, (**b**) 0° 400 °C 0.1 s^{-1}, (**c**) 0° 400 °C 0.001 s^{-1}, (**d**) 45° 400 °C 0.001 s^{-1}, (**e**) 90° 400 °C 0.001 s^{-1}.

Figure 6 shows the fracture morphology of the 6082 alloy under various tensile conditions. All the fracture surfaces present an obvious ductile fracture, and a large number of dimples were formed. After reaching the yield limit, the material exhibits necking. When subjected to tensile deformation at 400 °C and 0.1 s^{-1}, the fracture surface has a great amount of dimples, and the deep dimples are distributed uniformly, resulting in an enhancement of the plasticity and a drop of strength. When the tensile temperature declines to 300 °C and the condition is 0.1 s^{-1}, the number of dimples significantly decreases, the depth of the dimples becomes shallower and the distribution of the dimples is less uniform. As shown in Figure 6c, when tensiled at 0.001 s^{-1}, 400 °C, the number of the dimples gradually increases, and they are arranged tightly with overlapping and increasing in size and depth. From Figure 6c–e, the fractures of the samples from three directions appear with large dimples surrounded by small dimples, exhibiting excellent plasticity. When tensiled at higher temperatures and lower strain rates, the dimples are more dense, deeper and have better plasticity.

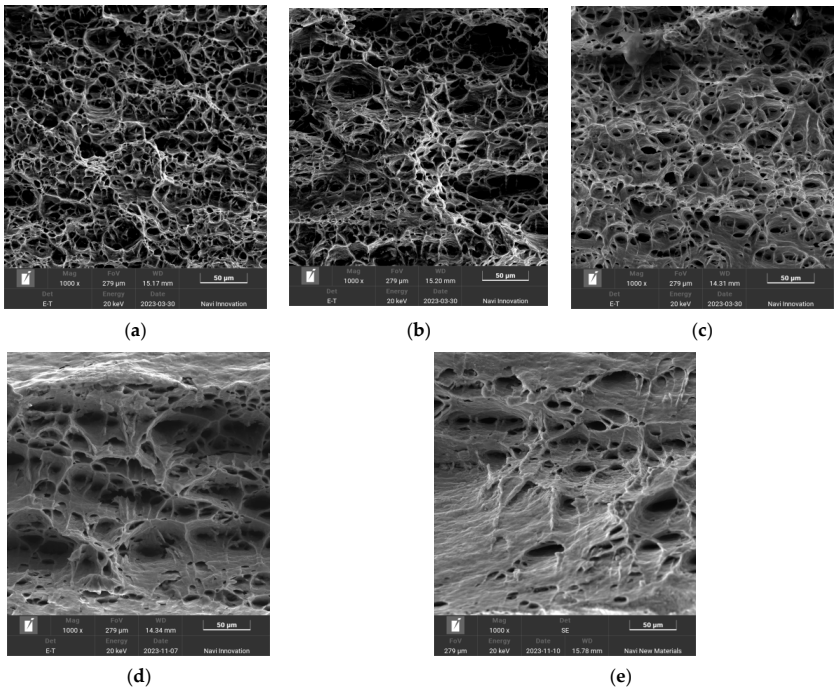

Figure 6. Fracture morphology of 6082 alloy under various conditions: (**a**) 0° 300 °C 0.1 s^{-1}, (**b**) 0° 400 °C 0.1 s^{-1}, (**c**) 0° 400 °C 0.001 s^{-1}, (**d**) 45° 400 °C 0.001 s^{-1}, (**e**) 90° 400 °C 0.001 s^{-1}.

4. Discussion

4.1. The Anisotropic Behavior

As shown in Figure 7, the microstructure of the extruded 6082 aluminum alloy along the extrusion direction. The microstructure is mainly a fibrous grain structure. The grain boundaries are well defined. The width of the grains was 20–50 µm. Previous studies imply that the fibrous grain structure can lead to the anisotropy of mechanical behavior [32,33]. Yang et al. [26] tested the compression behavior of Al-Zn-Mg-Cu alloy with a fibrous grain structure and deformation temperature ranges from 320 to 340 °C. It is found that the flow stress of 0° specimens ranks first, however, the corresponding values of the 90° specimen are the lowest. Ye et al. [27] explored the flow stress of Al-Mg-Si alloy at dynamic impact and claimed that the fibrous grains are the main reason that leads to the highest stress level of 0° specimens. It is widely accepted that the grain boundaries can impede the motion of dislocations; however, the fibrous grains lead to the various densities of grain boundaries in different direction samples. During the deformation, an extensive amount of dislocations will accumulate near the grain boundary, which results in the lattice distortion within the grain boundary, namely, grain boundary densities decide the effect of strengthening effect. Therefore, the different direction samples display anisotropic mechanical properties [34].

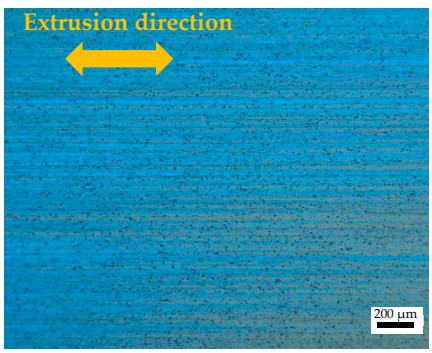

Figure 7. Grain structure of the original 6082 alloy.

It is necessary to consider the Schmid Factor and orientation distribution functions (ODFs) in the analysis of the anisotropic behavior [35], the equations are listed below:

$$\tau = \sigma_y = \frac{F}{A}\cos\phi\cos\lambda \tag{1}$$

$$M = \cos\phi\cos\lambda \tag{2}$$

where τ represents critical resolved shear stress, A represents loading section, ϕ represents angle between loading axis and the normal to slip plane, λ represents angle between loading axis to slip direction, σ_y represents yield stress, and M represents Schmid factor. Yang et al. [26] have tested and calculated the SF of an extruded Al-Zn-Mg-Cu alloy. The results show the Schmid Factor of 0° samples is lower than in other directions, and its flow stresses are the highest. Ye et al. [27] have tested and discussed the SF of an extruded Al-Mg-Si bar, the results indicate that the 45° sample owns the highest value of SF, and, accordingly, its stress levels are the lowest during dynamic impact loading tests.

Figure 8a is a schematic diagram of the orientation of the typical texture components, while Figure 8b shows the ODF sections for the 6082 sheet. The 6082 sheet exhibits an obvious Brass texture component. The Brass texture component is a typical deformation texture. Previous research has shown that deformation texture has a strengthening influence on the anisotropy of the sheet, while recrystallization texture has a weakening effect on anisotropy [36]. In non-recrystallized or partially recrystallized states, if there are strong deformation textures such as Brass {011}<211> in the alloy, it can cause significant anisotropy [37]. From Equation (2), it can be seen that the smaller the maximum Schmidt factor, the stronger the strengthening effect of texture on the tensile direction.

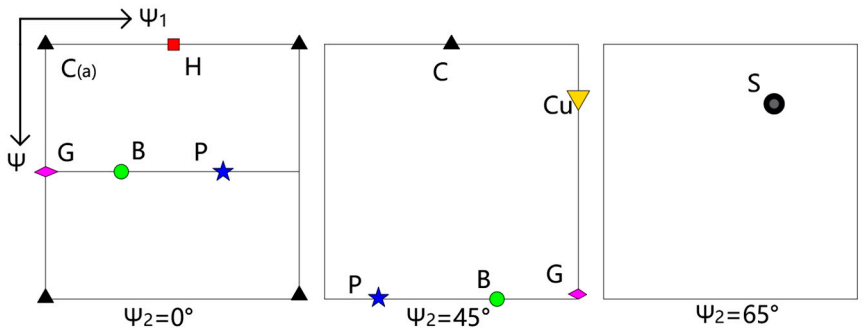

(**a**)

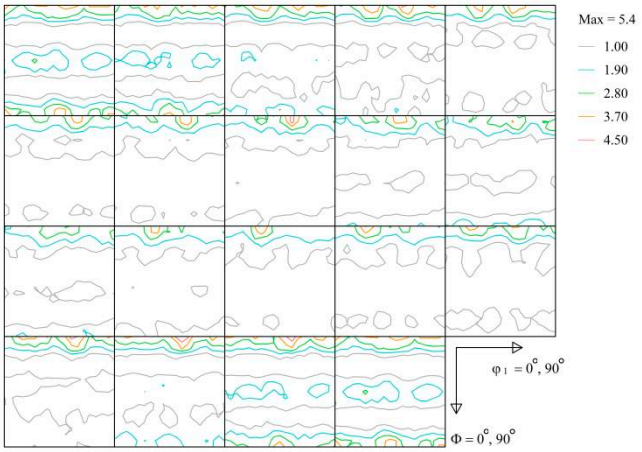

(**b**)

Figure 8. (**a**) Typical texture components in the ODF sections (φ_2 = 0°, φ_2 = 45°, φ_2 = 65°), (**b**) the ODF map of the 6082 sheet.

4.2. The Dynamic Softening Effects

Figure 9 shows the microstructure of the 6082 alloy under different deformation conditions. From Figure 9a–e, it is observed that during the tension, the grains undergo shear deformation along a 45° direction. The fracture path of the alloy is partially transgranular, partially intergranular, and dominated by transgranular fracture. Intergranular fracture mainly occurs in the recrystallized grains with weaker bonding ability. During the tensile process, when the strain becomes larger, the micropores inside the alloy nucleate and grow, and pores begin to aggregate, ultimately leading to the fracture, forming pores near the fracture surface. Additionally, under high-temperature tensile deformation conditions, different degrees of recrystallization occurred. The recrystallized grains are mainly distributed near the grain boundary, and the energy difference between both sides of the grain boundary acts as a driving force for recrystallization. Comparing Figure 9b to c, it can be seen that reducing the strain rate can improve the elongation of 6082 aluminum alloy. When tensiled at a low strain rate, the corresponding tensile time is longer, and the material has sufficient time to process dynamic recovery and dynamic recrystallization. The softening effects will improve the elongation of the material. Comparing Figure 9a to b, as tensiled at a higher temperature of 400 °C, the elongation of 6082 aluminum alloy is much better. As a kind of face-center cubic structure metal, aluminum alloy has considerable slip systems. The ductility of metals and alloys depends on the activation of slip systems. The high temperature will facilitate the diffusion of atoms, which can efficiently improve the plastic deformation ability of materials. Both temperature and strain rate have an impact on elongation.

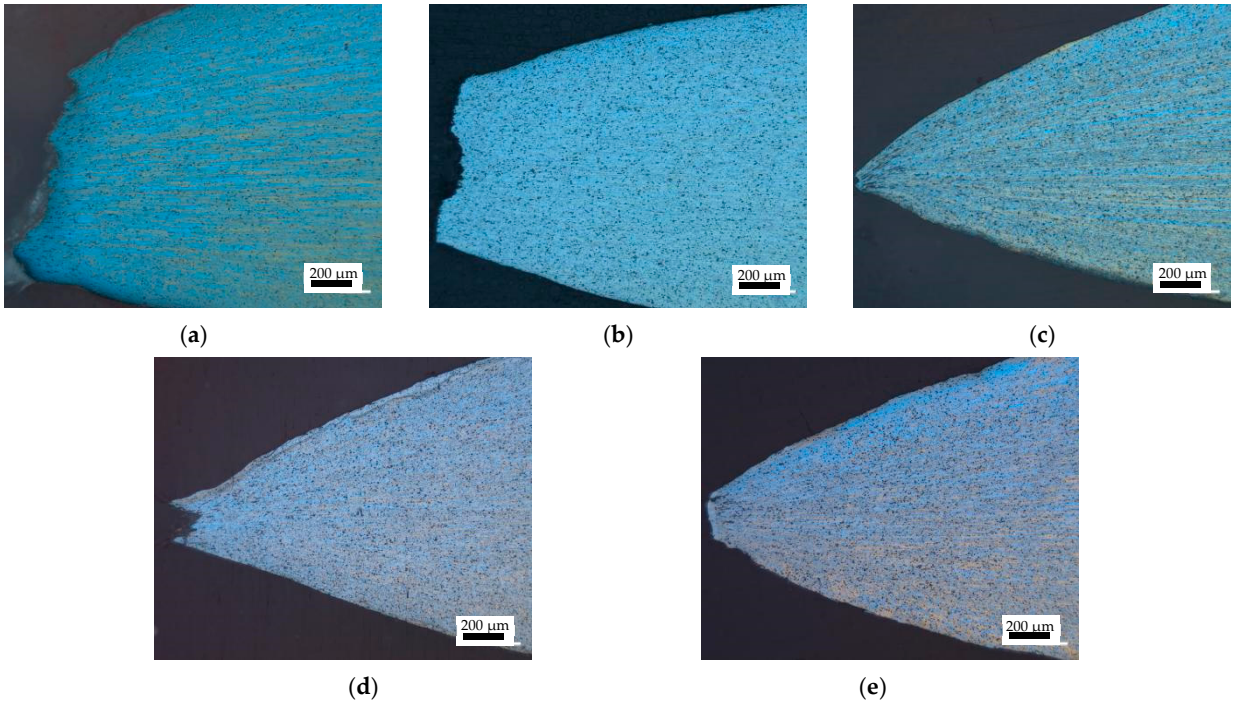

Figure 9. Microstructure of 6082 sheets after deformation: (**a**) 0° 300 °C 0.1 s^{-1}, (**b**) 0° 400 °C 0.1 s^{-1}, (**c**) 0° 400 °C 0.001 s^{-1}, (**d**) 45° 400 °C 0.001 s^{-1}, (**e**) 90° 400 °C 0.001 s^{-1}.

Figure 10 shows the TEM morphology of the 6082 alloy after tension at various conditions. During the tensile deformation process of the specimen, a certain amount of dislocations are generated in the matrix, as displayed in Figure 10a, when subjected to tensile deformation at 300 °C, 0.1 s^{-1}, the effect of dynamic recovery is relatively weaker, and dislocations can not be eliminated in time, causing the accumulation of dislocations and formation of high dislocation density regions. As the deformation temperature increases, at 400 °C and a strain rate of 0.1 s^{-1}, as can be seen in Figure 10b, the dynamic recovery

effects are more significant, and a drop in dislocation density was observed. Further, the polygonized dislocation cells that appear in the matrix and the alloy exhibit typical recovery characteristics. As the strain rate decreases, at 400 °C and a strain rate of 0.001/s, the deformation time is relatively longer, the dynamic recovery is relatively obvious, and the dislocation density decreases rapidly (Figure 10c), and the dislocation cells are polygonized to form subgrains, the equiaxed grains are observed with clear grain boundaries, which implies the occurrence of recrystallization. Meanwhile, under relatively high deformation temperature and low strain rate conditions (400 °C, 0.001/s), as displayed in Figure 10c–e, there is no obvious difference in dislocation density and distribution among samples in three different directions. The dislocation density inside the material is relatively low. Therefore, the effect of dislocation strengthening is weak, which is one of the reasons why the strength decreases with increasing temperature.

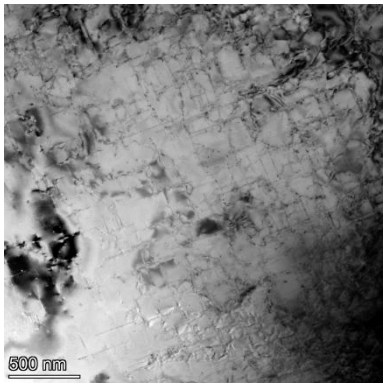

(**a**) 0° 300 °C 0.1/s

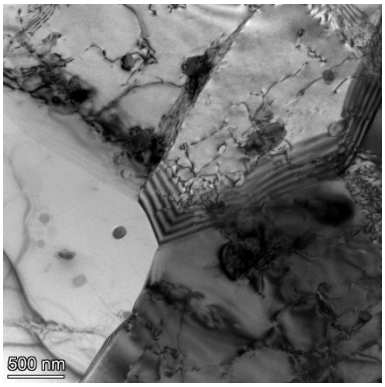

(**b**) 0° 400 °C 0.1/s

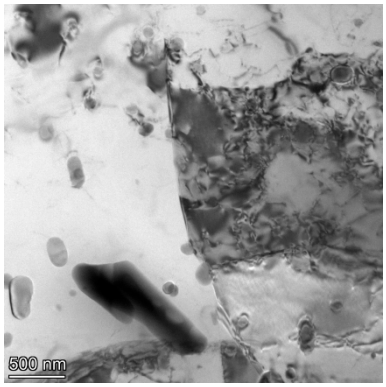

(**c**) 0° 400 °C 0.001/s

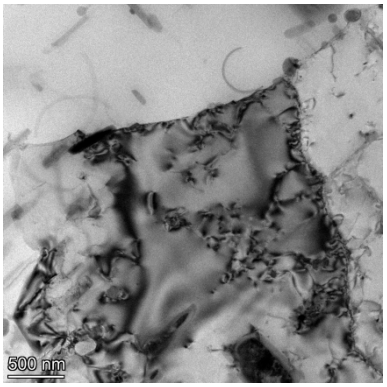

(**d**) 45° 400 °C 0.001/s

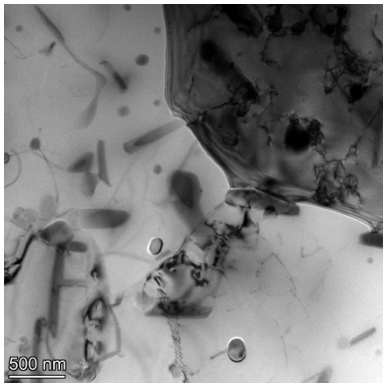

(**e**) 90° 400 °C 0.001/s

Figure 10. TEM images of 6082 alloy after tension: (**a**) 0° 300 °C 0.1 s^{-1}, (**b**) 0° 400 °C 0.1 s^{-1}, (**c**) 0° 400 °C 0.001 s^{-1}, (**d**) 45° 400 °C 0.001 s^{-1}, (**e**) 90° 400 °C 0.001 s^{-1}.

Furthermore, the size and shape of precipitates are also important for the strength during thermal deformation. Based on the classic strengthening theory of metals [38,39], there are two mechanisms between dislocations and precipitate during alloy deformation, there are cutting and bypassing. When the precipitate is small in size and maintains a coherent relationship with the matrix, dislocations are mainly cut through the precipitates. When the size of the precipitate is larger or no longer keeps a coherent relationship, the dislocation bypasses the precipitate. The strength of an alloy depends on the resistance to the interaction between precipitate and dislocations during the tensile process [40]. When dislocations cut through precipitates, the resistance is higher than that of the bypass mechanism. Therefore, the smaller the size of precipitates in the alloy and the more coherent precipitates it contains, the dislocations need to cut through more precipitates, and the higher the strength. When tensiled at 300 °C, as shown in Figure 10a, the needle-like precipitate is observed, it will impede the motion of dislocation and enhance the deformation resistance of the material. When deformed at higher temperatures, as shown in Figure 10b,c, the density of needle-like precipitate decreases, rod-shaped precipitates appear in the matrix, the higher the tensile temperature, the more significant the precipitate coarsening, and the pinning effect of the coarse precipitate is weaker, which cannot offset the softening effect caused by temperature increase. Therefore, as the temperature increases and the strain rate decreases, the strength of the alloy decreases.

5. Conclusions

(1) The strength of the extruded 6082 aluminum alloy declines with increasing tensile temperature and decreasing strain rate. The alloy displays ductile fracture. A certain amount of dimples appear at the fracture surface. When stretched at higher temperatures and lower strain rates, the number of dimples increases. The depth of the dimples became deep, and the plasticity of the alloy was improved.

(2) When deformed at 300 °C, the dynamic recovery occurs. The density of dislocation drops with the increasing temperature and decreasing strain rate. In addition, when deformed at 400 °C, some equiaxed grains are observed, which indicates a dynamic recrystallization. Meanwhile, the phenomenon of precipitate coarsening is observed. The dynamic recovery, dynamic recrystallization and precipitate coarsening result in a decline in the stress level of the alloy.

(3) The extruded 6082 alloy exhibits a mechanical anisotropy at the tensile temperature of 300 °C. This can attributed to the fibrous grains and Brass component. As the temperature rises to a temperature of 400 °C, there is no obvious anisotropy. Because the slip is easier to activate, the dynamic recrystallization leads to the evolution of grain shape and texture.

Author Contributions: Conceptualization, S.Q. and T.Y.; Methodology, Y.W. and W.L.; Data curation, J.L. and L.L.; Validation, J.T. and W.L.; Visualization J.L. and L.L.; Formal analysis, T.Y. and Y.W.; Funding acquisition, Y.W.; Investigation, T.Y. and E.X.; Resources, J.T. and L.L.; Supervision Y.W.; Writing—original draft, S.Q. and E.X.; Writing—review and editing, W.L. and Y.W. All authors have read and agreed to the published version of the manuscript.

Funding: The research described in this paper was supported by the National Natural Science foundation of China (52201074, 52171115), the Scientific Research Fund of Hunan Provincial Education Department of China (22A0626, 22B0867), the Scientific Research Project of Hunan Institute of Technology (grant number HQ23023), and Aid Program for Science and Technology Innovative Research Team in Higher Educational Institutions of Hunan Province.

Institutional Review Board Statement: Not applicable.

Informed Consent Statement: Not applicable.

Data Availability Statement: Data is contained within the article.

Conflicts of Interest: The authors declare no conflict of interest.

References

1. Zhang, W.; Xu, J. Advanced lightweight materials for automobiles: A review. *Mater. Design* **2022**, *221*, 110994. [CrossRef]
2. Georgantzia, E.; Gkantou, M.; Kamaris, G.S. Aluminium alloys as structural material: A review of research. *Eng. Struct.* **2021**, *227*, 111372. [CrossRef]
3. Li, S.S.; Yue, X.; Li, Q.Y.; Peng, H.L.; Dong, B.X.; Liu, T.S.; Jiang, Q.C. Development and applications of aluminum alloys for aerospace industry. *J. Mater. Res. Technol.* **2023**, *27*, 944–983. [CrossRef]
4. Blanco, D.; Rubio, E.M.; Lorente-Pedreille, R.M.; Sáenz-Nuño, M.A. Sustainable processes in aluminium, magnesium, and titanium alloys applied to the transport sector: A review. *Metals* **2021**, *12*, 9. [CrossRef]
5. Berlanga-Labari, C.; Biezma-Moraleda, M.V.; Rivero, P.J. Corrosion of cast aluminum alloys: A review. *Metals* **2020**, *10*, 1384. [CrossRef]
6. Xu, X.; Zhu, W.; Guo, X.; Liang, C.; Deng, Y. Effect of ageing treatment process on the microstructure development and mechanical properties of 6082 Al alloy. *J. Alloys Compd.* **2023**, *935*, 167892. [CrossRef]
7. Kumar, N.; Jayaganthan, R.; Brokmeier, H.G. Effect of deformation temperature on precipitation, microstructural evolution, mechanical and corrosion behavior of 6082 Al alloy. *Trans. Nonferrous Metal. Soc.* **2017**, *27*, 475–492. [CrossRef]
8. Hu, Z.; Zheng, J.; Pang, Q.; Sun, Q.; Zhao, N. Influence of strain rates and aging time on microstructure and hardness of integrally compressed 6082 aluminum alloy. *J. Mater. Res. Technol.* **2023**, *27*, 826–838. [CrossRef]
9. Deng, L.; Zhang, H.D.; Li, G.A.; Tang, X.F.; Yi, P.S.; Liu, Z. Processing map and hot deformation behavior of squeeze cast 6082 aluminum alloy. *Trans. Nonferrous Metal. Soc.* **2022**, *32*, 2150–2163. [CrossRef]
10. Leśniak, D.; Zasadziński, J.; Libura, W.; Żaba, K.; Puchlerska, S.; Madura, J.; Jurczak, H. FEM Numerical and Experimental Study on Dimensional Accuracy of Tubes Extruded from 6082 and 7021 Aluminium Alloys. *Materials* **2023**, *16*, 556. [CrossRef]
11. Noga, P.; Piotrowicz, A.; Skrzekut, T.; Zwoliński, A.; Strzępek, P. Effect of Various Forms of Aluminum 6082 on the Mechanical Properties, Microstructure and Surface Modification of the Profile after Extrusion Process. *Materials* **2021**, *14*, 5066. [CrossRef] [PubMed]
12. Peruš, I.; Kugler, G.; Malej, S.; Terčelj, M. Contour maps for simultaneous increase in yield strength and elongation of hot extruded aluminum alloy 6082. *Metals* **2022**, *12*, 461. [CrossRef]
13. Hua, L.; Yuan, P.G.; Zhan, N.; Hu, Z.L.; Ma, H.J. Microstructure and mechanical properties of 6082 aluminum alloy processed by preaging and hot forging. *Trans. Nonferrous Metal. Soc.* **2022**, *32*, 790–800. [CrossRef]
14. Noga, P.; Skrzekut, T.; Wędrychowicz, M.; Węglowski, M.S.; Węglowska, A. Research of friction stir welding (FSW) and electron beam welding (EBW) process for 6082-T6 aluminum alloy. *Materials* **2023**, *16*, 4937. [CrossRef] [PubMed]
15. Hu, D.; Wang, L.; Wang, H. Dynamic recrystallization behavior and processing map of the 6082 aluminum alloy. *Materials* **2020**, *13*, 1042. [CrossRef] [PubMed]
16. Li, K.; Pan, Q.; Li, R.; Liu, S.; Huang, Z.; He, X. Constitutive modeling of the hot deformation behavior in 6082 aluminum alloy. *J. Mater. Eng. Perform.* **2019**, *28*, 981–994. [CrossRef]
17. Yang, Q.Y.; Yang, D.; Zhang, Z.Q.; Cao, L.F.; Wu, X.D.; Huang, G.J.; Liu, Q. Flow behavior and microstructure evolution of 6A82 aluminium alloy with high copper content during hot compression deformation at elevated temperatures. *Trans. Nonferrous Metal. Soc.* **2016**, *26*, 649–657. [CrossRef]
18. Hidalgo-Manrique, P.; Cao, S.; Shercliff, H.R.; Hunt, R.D.; Robson, J.D. Microstructure and properties of aluminium alloy 6082 formed by the Hot Form Quench process. *Mater. Sci. Eng. A* **2021**, *804*, 140751. [CrossRef]
19. Zheng, J.H.; Pruncu, C.; Zhang, K.; Zheng, K.; Jiang, J. Quantifying geometrically necessary dislocation density during hot deformation in AA6082 Al alloy. *Mater. Sci. Eng. A* **2021**, *814*, 141158. [CrossRef]
20. Zhao, N.; Sun, Q.; Pang, Q.; Hu, Z. Comprehensive study of hot compression behaviors and microstructure evolution of solutionized 6082 aluminum alloy extruded bar. *J. Alloys Compd.* **2023**, *931*, 167541. [CrossRef]
21. Xu, Z.; Ma, H.; Zhao, N.; Hu, Z. Investigation on compressive formability and microstructure evolution of 6082-T6 aluminum alloy. *Metals* **2020**, *10*, 469. [CrossRef]
22. Chen, Y.; Clausen, A.H.; Hopperstad, O.S.; Langseth, M. Stress–strain behaviour of aluminium alloys at a wide range of strain rates. *Int. J Solids. Struct.* **2009**, *46*, 3825–3835. [CrossRef]
23. Chakraborty, P.; Singha, M.K.; Tiwari, V. Anisotropic mechanical response of AA7475-T7351 alloy at different loading rates and temperatures. *Thin Wall Struct.* **2023**, *188*, 110842. [CrossRef]
24. Barnwal, V.K.; Raghavan, R.; Tewari, A.; Narasimhan, K.; Mishra, S.K. Effect of microstructure and texture on forming behaviour of AA-6061 aluminium alloy sheet. *Mater. Sci. Eng. A* **2017**, *679*, 56–65. [CrossRef]
25. Fan, X.; Li, Y.; Xu, C.; Wang, B.; Peng, R.; Chen, J. Improved mechanical anisotropy and texture optimization of a 3xx aluminum alloy by differential temperature rolling. *Mater. Sci. Eng. A* **2021**, *799*, 140278. [CrossRef]
26. Yang, Y.; Xie, Z.P.; Zhang, Z.; Li, X.; Wang, Q.; Zhang, Y. Processing maps for hot deformation of the extruded 7075 aluminum alloy bar: Anisotropy of hot workability. *Mater. Sci. Eng. A* **2014**, *615*, 183–190. [CrossRef]
27. Ye, T.; Li, L.X.; Liu, X.; Liu, W.H.; Guo, P.C.; Tang, X. Anisotropic deformation behavior of as-extruded 6063-T4 alloy under dynamic impact loading. *Mater. Sci. Eng. A* **2016**, *666*, 149–155. [CrossRef]
28. Frodal, B.H.; Thomesen, S.; Børvik, T.; Hopperstad, O.S. On fracture anisotropy in textured aluminium alloys. *Int. J. Solids Struct.* **2022**, *244*, 111563. [CrossRef]

29. Thomesen, S.; Hopperstad, O.S.; Børvik, T. Anisotropic plasticity and fracture of three 6000-series aluminum alloys. *Metals* **2021**, *11*, 557. [CrossRef]
30. Attarilar, S.; Ebrahimi, M.; Hsieh, T.H.; Uan, J.Y.; Göde, C. An insight into the vibration-assisted rolling of AA5052 aluminum alloy: Tensile strength, deformation microstructure, and texture evolution. *Mater. Sci. Eng. A* **2021**, *803*, 140489. [CrossRef]
31. Ye, T.; Xia, E.L.; Qiu, S.; Wang, Y.; Yue, H.Y.; Liu, J.; Wu, Y. High-temperature tensile mechanical properties and microstructure of rolled 6082-T6 aluminum alloy sheets. *Materials* **2023**, *16*, 7019. [CrossRef] [PubMed]
32. Naumenko, K.; Gariboldi, E. Experimental analysis and constitutive modeling of anisotropic creep damage in a wrought age-hardenable Al alloy. *Eng. Fract. Mech.* **2022**, *259*, 108119. [CrossRef]
33. Cho, K.K.; Chung, Y.H.; Lee, C.W.; Kwun, S.I.; Shin, M. Effects of grain shape and texture on the yield strength anisotropy of Al-Li alloy sheet. *Scr. Mater.* **1999**, *40*, 651–657. [CrossRef]
34. Lim, H.; Lee, M.G.; Kim, J.H.; Adams, B.L.; Wagoner, R.H. Simulation of polycrystal deformation with grain and grain boundary effects. *Int. J. Plast.* **2011**, *27*, 1328–1354. [CrossRef]
35. Raabe, D.; Roters, F. Using texture components in crystal plasticity finite element simulations. *Int. J. Plast.* **2004**, *20*, 339–361. [CrossRef]
36. Zhou, Y.; Wang, L.; Chen, H.; Liu, J.; Dan, C.; Ma, S.; Chen, Z. Enhancing mechanical properties and improving mechanical anisotropy of rolled 2024 Al sheet by TiB_2 nanoparticles. *Mater. Sci. Eng. A* **2023**, *874*, 145077. [CrossRef]
37. Li, Y.; Xu, G.; Liu, S.; Wang, B.; Peng, X. Study on anisotropy of Al-Zn-Mg-Sc-Zr alloy sheet. *Mater. Charact.* **2021**, *172*, 110904. [CrossRef]
38. Fomin, E.V.; Mayer, A.E.; Krasnikov, V.S. Prediction of shear strength of cluster-strengthened aluminum with multi-scale approach describing transition from cutting to bypass of precipitates by dislocations. *Int. J. Plast.* **2021**, *146*, 103095. [CrossRef]
39. Gao, R.; Li, Y.; Li, Z.; Li, X.; Wen, K.; Zhang, Y.; Xiong, B. Quantitative relationship between microstructure and tensile properties of Al-Zn-Mg-Cu alloys with various alloying degrees. *J. Mater. Res. Technol.* **2022**, *18*, 5394–5405. [CrossRef]
40. Zhao, X.; Liu, W.; Xiao, D.; Ma, Y.; Huang, L.; Tang, Y. A critical review: Crystal structure, evolution and interaction mechanism with dislocations of nano precipitates in Al-Li alloys. *Mater. Des.* **2022**, *217*, 110629. [CrossRef]

Disclaimer/Publisher's Note: The statements, opinions and data contained in all publications are solely those of the individual author(s) and contributor(s) and not of MDPI and/or the editor(s). MDPI and/or the editor(s) disclaim responsibility for any injury to people or property resulting from any ideas, methods, instructions or products referred to in the content.